ATLAS Internal Note
PHYS-NO-068
26 July 1995

HIGGS-BOSON STUDY AT HIGH MASS AT THE LHC

E.G. Boos, N.S. Pokrovski, B.O. Zhautykov
Inst. of High-Energy Phys. of the Nat. Acad. of Sci. Kazakhstan, Almaty

ATLAS Collaboration

1 INTRODUCTION

After the heavy vector boson [1] and the t-quark [2] discovery, the search for the heavy scalar H_0 boson is the central problem for electroweak force unification [3]. The mass interval of this object is limited up to 1000 GeV [4] by theoretical evaluation, and lower (> 65 GeV [5]) by accelerator experiments at FNAL [6] and CERN [7].

At the hadron collider the main channels of Higgs-boson production are the reactions of gluon ($gg \to H_0$), and heavy vector boson ($W^+W^- \to H_0, ZZ \to H_0$) fusion; the estimated production cross-section for mass $m_H \simeq 500$ GeV is of the order of 10 pb. Ultimately, for large masses the competitive channel is the vector boson bremsstrahlung ($q\bar{q} \to WH$), but the cross-section itself decreases up to a value ~ 1 pb. When the 'gold' mode of Higgs-boson decay of four charged leptons ($H \to ZZ \to 4\ell$) amounts to 3×10^{-4} [8], the problem of optimal suppression of background reactions is of great importance. The additional complication of this problem is connected with the growth of the width of the H-resonance in the mass range higher than the threshold production of the $t\bar{t}$-pair ($\Gamma_H G = 350$ GeV, Fig. 1 [8, 9]).

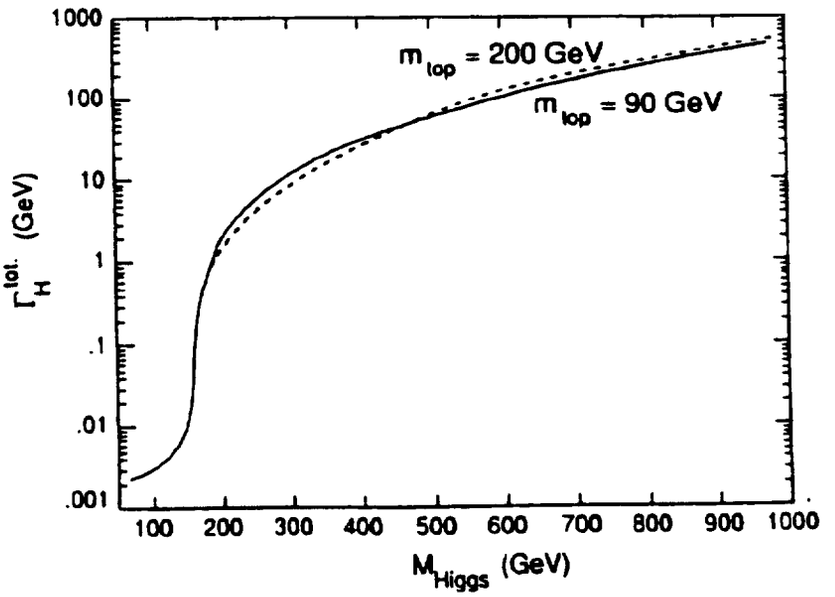

Figure 1: Variation of the Higgs total width versus m_H [8].

In the present study a new approach to the selection of the candidates of Higgs bosons for the reaction $H \to 2\, e^+\, (\mu^+)\, 2\, e^-(\mu^-)$ with effective suppression of background is suggested. In our analysis we recognize the fact that in the decay of the scalar Higgs into two vector bosons correlations between the two Z's and hence the boson leptons are introduced. Such a correlation cannot be exploited with a simple kinematical cut.

In contrast to the traditional method of background suppression by means of pseudorapidities and transversal momentum cuts, we consider a method in which intrinsic correlation of the secondary leptons and complete kinematical information is used in the multidimensional phase space. In this case the ranges with high-density events (clusters) are separated on the basis of additional criteria with respect to the invariant properties of the decay, P-symmetry and also the invariance with respect to the three-dimensional

rotation of the events. Simple applications of this method have been applied previously in analysis of $\bar{p}p$-interactions at 32 GeV [10].

2 DESCRIPTION OF THE METHOD

2.1 The minimal spanning tree

Let us put many points (events) in multidimentional phase space (in our case 4n = 16) and evaluate the distance for every pair $(A; B)$ of events as

$$d^{(AB)} = -\sum_{i-1}^{n}[p_i^{4(A)} - p_i^{4(B)}]^2 \,. \tag{1}$$

The line $d^{(AB)}$ connecting two arbitrary $(A; B)$ points will be called the branch [11]. Then the minimal spanning tree is the unique configuration (Fig. 2) from $(N-1)$ branches, connecting all points (N being the number of the complete events) such that branch lengths are minimized. The tree construction begins at an arbitrary point (No. 1). The nearest event to this point is found (No. 2) and the subtree formed with a unique $[d^{(1,2)}]$ branch. Subsequently, the next closest point to one of the events ($N1$ or $N2$) is found and added to the subtree. This procedure of searching for the nearest point (event) and adding it to the subtree must be continued until all of the N points are connected [12].

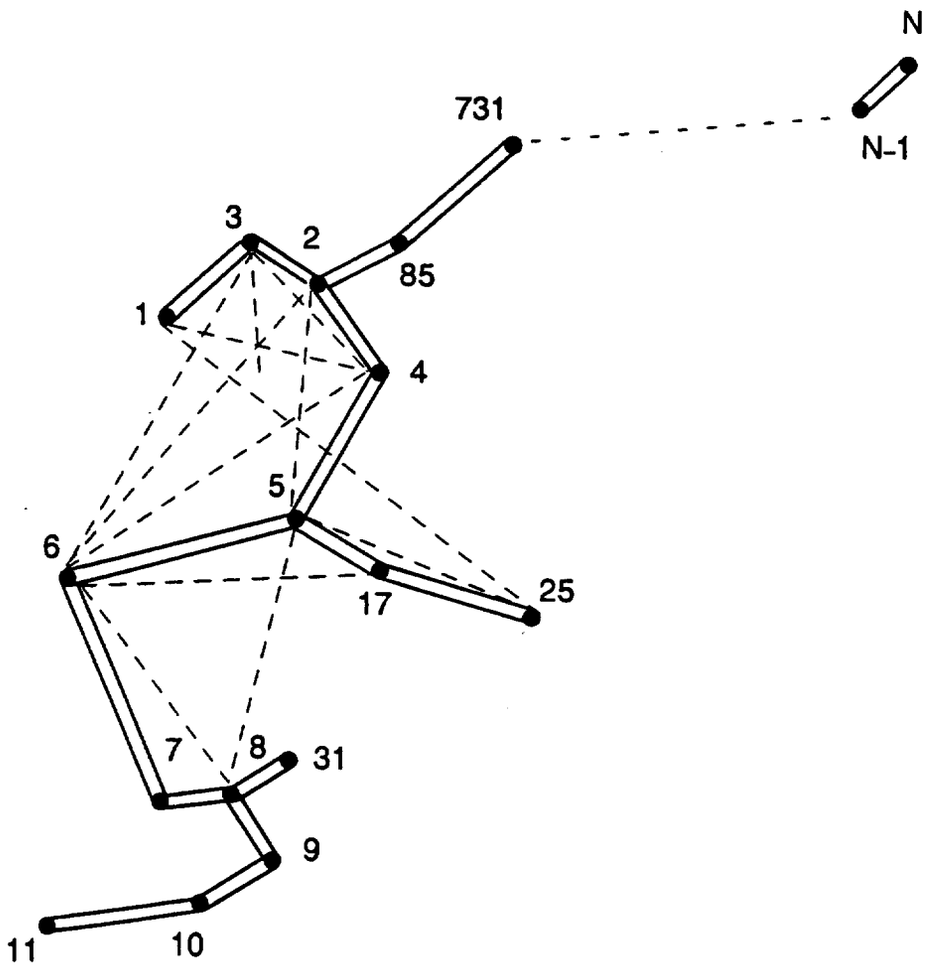

Figure 2: Schema of the minimal spanning tree.

We shall now give details of branch minimization:

i) in the $d^{(AB)}$ calculation only four vectors for identical particles can be substracted;

ii) if inside the events many identical particles exist, possible combinations must be considered and minimal $d^{(AB)}$ stored;

iii) after establishing the minimal branch length, the track number in the new sample must be given the same numbering as its predecessor (track ordering);

iv) the three-dimensional rotation of events must minimize the branch length between two events (A; B) without changing the internal distances between the particles.

For particles of the same nature Eq. (1) can be rewritten in the following way:

$$d^{(AB)} = d_p^{(AB)} - d_E^{(AB)} = \sum_{i=1}^{n} (\vec{p}_i^{\,A} - \vec{p}_i^{\,B})^2 - \sum_{i=1}^{n} (E_i^A - E_i^B)^2 \,. \tag{2}$$

Let us introduce a real orthogonal matrix R to minimize $d_p^{(AB)}$ and introduce the impulses of the particles as $(3 \times n)$ dimensional matrices

$$A = \begin{pmatrix} p_{x_1}^A & p_{x_2}^A & \dots & p_{x_n}^A \\ p_{y_1}^A & p_{y_2}^A & \dots & p_{y_n}^A \\ p_{z_1}^A & p_{z_2}^A & \dots & p_{z_n}^A \end{pmatrix} , \qquad B = \begin{pmatrix} p_{x_1}^B & p_{x_2}^B & \dots & p_{x_n}^B \\ p_{y_1}^B & p_{y_2}^B & \dots & p_{y_n}^B \\ p_{z_1}^B & p_{z_2}^B & \dots & p_{z_n}^B \end{pmatrix} . \tag{3}$$

Then

$$d_{\min}^{(AB)} = tr[(A - RB)^T (A - RB)] - d_E \,. \tag{4}$$

After simple transformation

$$\begin{aligned} d_p^{(AB)} &= tr[(A - R \times B)^T (A - RB)] \\ &= \sum_{i=1}^{n} [(\vec{p}_i^{\,A})^2 - (\vec{p}_i^{\,B})^2] - 2 \times tr\,(BA^T R) \,. \end{aligned} \tag{5}$$

To minimize $d_p^{(AB)}$, $tr(BA^T R)$ should be maximized.
Let us consider the polar expansion of the matrix [14]

$$BA^T = U = PQ \,, \tag{6}$$

where P is a symmetric matrix ($P = P^T$) and Q is the orthogonal matrix ($Q\ Q^T = 1$). The maximum of the trace $tr(BA^T R) = tr(PQR)$ is achieved at $QR \equiv 1$. Then

$$d_{\min}^{(AB)} = \sum_{i=1}^{n} [(\vec{p}_i^{\,A})^2 + (\vec{p}_i^{\,B})^2] - 2tr\ P - \sum_{i=1}^{n} [(E_i^A)^2 - (E_i^B)^2] \,, \tag{7}$$

where $tr\ P = \sum_{j=1}^{3} \lambda_j$, λ_j are the eigenvalues of the symmetric matrix P.
Equation (7) can be rewritten as

$$d_{\min}^{(A,B)} = 2\left[\sum_{i=1}^{n} E_i^A \times E_i^B - \sum_{i=1}^{n} m_i^2 - \sum_{j=1}^{3} \lambda_j\right] . \tag{8}$$

Taking into account that

$$UU^T = (PQ)(PQ)^T = P^2 \tag{9}$$

and that $tr\ P^2 = \sum_{j=1}^{3} \lambda_j^2$, we obtain the equations for the estimation of $x = \sum_{j=1}^{3} \lambda j$. Following the properties of the square matrices

$$tr\ P^2 = \sum_{j=1}^{3} \lambda_j^2 = \lambda_1^2 + \lambda_2^2 + \lambda_3^2 = a \tag{10}$$

$$det\ P^2 = \lambda_1^2 \times \lambda_2^2 \times \lambda_3^2 = b\,, \tag{11}$$

and

$$W_{11} \times W_{22} - W_{12}^2 + W_{11} \times W_{33} - W_{13}^2 + W_{22} \times W_{33} - W_{23}^2 = \\ = \lambda_1^2 \times \lambda_2^2 + \lambda_1^2 \times \lambda_3^2 + \lambda_2^2 \times \lambda_3^2 = c\,, \tag{12}$$

where c is the sum of minors of the P^2 matrix, a, b, and c can therefore be calculated from the matrix

$$P^2 = (BA^T)(BA^T)^T = BA^T AB^T \tag{13}$$

in which the complete kinematical information about the two events $(A;\ B)$ is considered.

Solving Eqs. (10, 11) and (12) we can find a simple analytical solution for x:

$$x = a + 2\sqrt{c + 2\sqrt{b} \times x}\,, \tag{14}$$

which can be solved numerically with good accuracy in (6–8) iterations.

It should be pointed out that in the states with identical particles, the minimal distance $d_{\min}^{(A,B)}$ naturally selects the tracks in such a way that the ordering of identical particles arises synchronously in all of the included events.

In this case, distribution of one and the same physical quantity could be quite different for identical particles with different numbers within the event.

Using this method for CP symmetric final states it is possible to minimize $d_{\min}^{(A,B)}$ by CP violation of one of the considered samples. It should be especially noted that noticeable differences in the number of transformed and untransformed events can be indicative of the CP symmetry violation.

2.2 Clusterization of events

The analysis is as follows: after particle-ordering inside each event (sample) and 'minimal spanning tree' construction we introduce for each i-th event a term 'halo', with radius $d_i(k)$ covering 'k' nearest events ('neighbours'). Fixing 'k', the halo density is inversely proportional to $d_i(k)$. We also introduce a critical radius 'R' and consider as 'dense' those events for which $d_i(k) < R$ [12].

Then we arrange all events according to $d_i(k)$ proportional to decreasing density by 'k' constant ($k = 5$ [13]).

If in the halo density ordering of the i-th event a dense sample appears (j-th event) we combine them into a group with the name 'cluster'. The clusters grow step-by-step. If in the l-th event we do not find amongst its neighbours the dense events considered before, we consider it as a parent of a new cluster. For dense events included in one cluster, we consider all samples from its halo as a shell of border events to this cluster. In this way we could find an event in which halo samples belong to different clusters. In

this case we look at the populations of each cluster. If one of them contains less then N_0 (clusterization parameter) events, they must be fused into one cluster and all the border samples from previous different shells create one shell around them. But if in both clusters the population is greater than N_0, they must be considered separately. Events maintaining two samples in the halo indicate a 'valley' between these two clusters.

An event in which a halo of dense events is absent cannot be considered further. In this way many clusters can appear when considering the complete statistics.

3 The results

This method was examined by events generated with the PYTHIA [15] program for pp interactions at LHC energy.

Considering branches for the 'golden' decay mode $H \to ZZ \to (e^+e^-)(e^+e^-)$, the cross-section responsible for Higgs-boson decay in 2 Z is presented in Table 1 for two Higgs-mass intervals: 325 GeV $\leq m_H <$ 475 GeV ($m_H = 400$ GeV), and 400 GeV $< m_H <$ 600 GeV ($m_H = 500$ GeV).

As background all reactions with two independent Z bosons in the final state were considered [15]. According to the diagrams considered in PYTHIA, the background cross-section is greater than for the summary effect (column 6 in Table 1).

Table 1: $\sigma(fn[15])$

m_{H_0} (GeV)	$\sigma(gg \to H)$ $\times$ Br $(H \to 4\ell)$	$\sigma(W^+W^- \to H)$ $\times$ $Br(H \to 4\ell)$	$\sigma(ZZ \to H)$ $\times$ Br $(H \to 4\ell)$	Σ	$\sigma_{\text{back}}/\sigma_{\text{effect}}$
400	1.3b	0.23	0.09	1.68	1.5
500	0.55	0.15	0.05	0.75	2.0

In each mass interval of Higgs bosons 2000 events were generated. According to Table 1 the number of generated background events was 3000 and 4000, respectively. For Higgs boson decay the initial numbering of tracks was used as follows:

$$H \to Z^1\ (\ell_1^+\ell_1^-)\ Z^2\ (\ell_2^+\ell_2^-)\ . \tag{15}$$

As we do not know the true numbering we begin by considering randomly all possible permutations of the track positions. Subsequently, we build the minimal spanning tree and start the clusterization algorithm. It should be noted that the minimal distance ($d^{\min}_{A,B}$) analysis is invariant with respect to the rotation of events and its mirror image.

In the $d^{(AB)}$ minimization the following permutations are possible

$$\begin{aligned}
p_1 &= (\ell_1^+\ell_1^-,\ \ell_2^+\ell_2^-) - \text{true ordering}\ , \\
p_2 &= (\ell_2^+\ell_2^-,\ \ell_1^+\ell_1^-) - Z \text{ exchange}\ , \\
p_3 &= (\ell_2^+\ell_1^-,\ \ell_1^+\ell_2^-) - \text{exchange of positron}\ , \\
p_4 &= (\ell_1^+\ell_2^-,\ \ell_2^+\ell_1^-) - \text{exchange of electron}\ .
\end{aligned}$$

For charge conjugation

$$\begin{aligned}
p_5 &= (\ell_1^-\ell_1^+;\ \ell_2^-\ell_2^+) \\
p_6 &= (\ell_2^-\ell_2^+;\ \ell_1^-\ell_1^+) \\
p_7 &= (\ell_2^-\ell_1^+;\ \ell_1^-\ell_2^+) \\
p_8 &= (\ell_1^-\ell_2^+;\ \ell_2^-\ell_1^+)\ .
\end{aligned}$$

Remembering the initial numbering we can perform the analysis of the permutations selected during the construction of the spanning tree. In Fig. 3 the number of such permutation is given for true Higgs events and background events. From that picture it follows that the true Z ordering or change of its position is quite the same, but the tree construction practically excludes the permutation of leptons between Z 'parents' in the true Higgs events and significantly suppresses it in the background events.

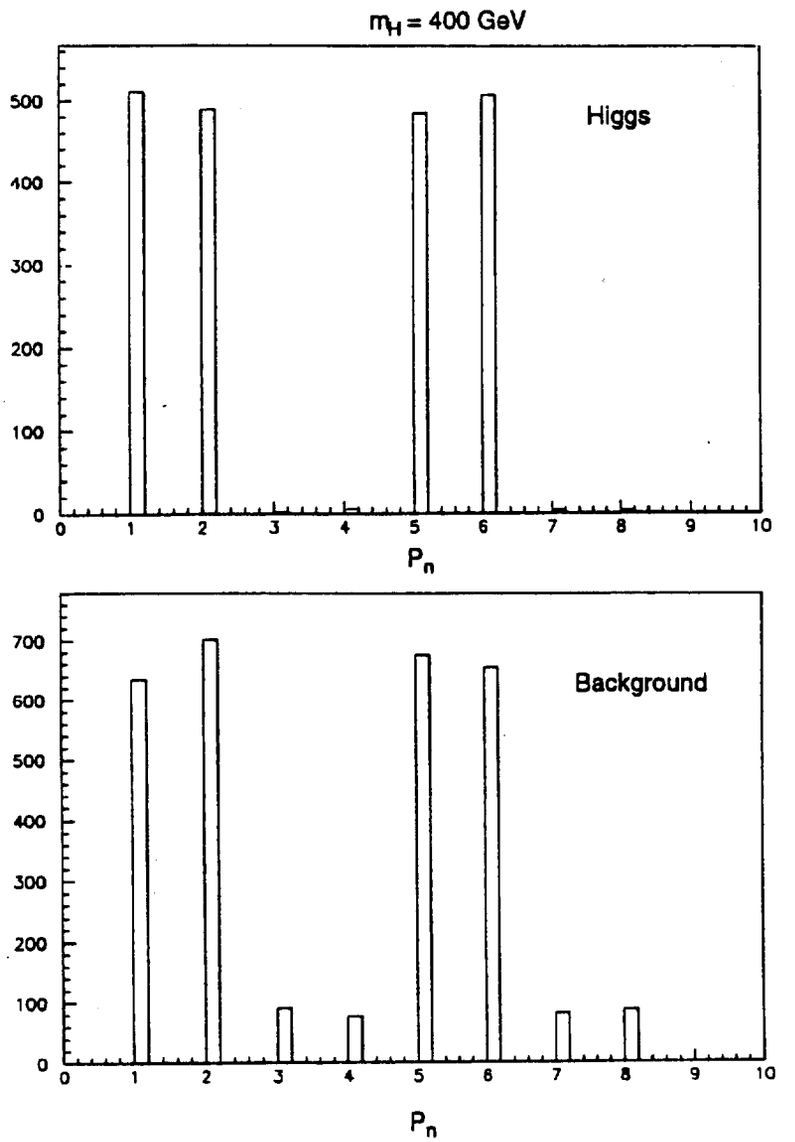

Figure 3a: The combination distribution for Higgs events (top) and background ones (bottom) at $m_H = 400$ GeV/c^2.

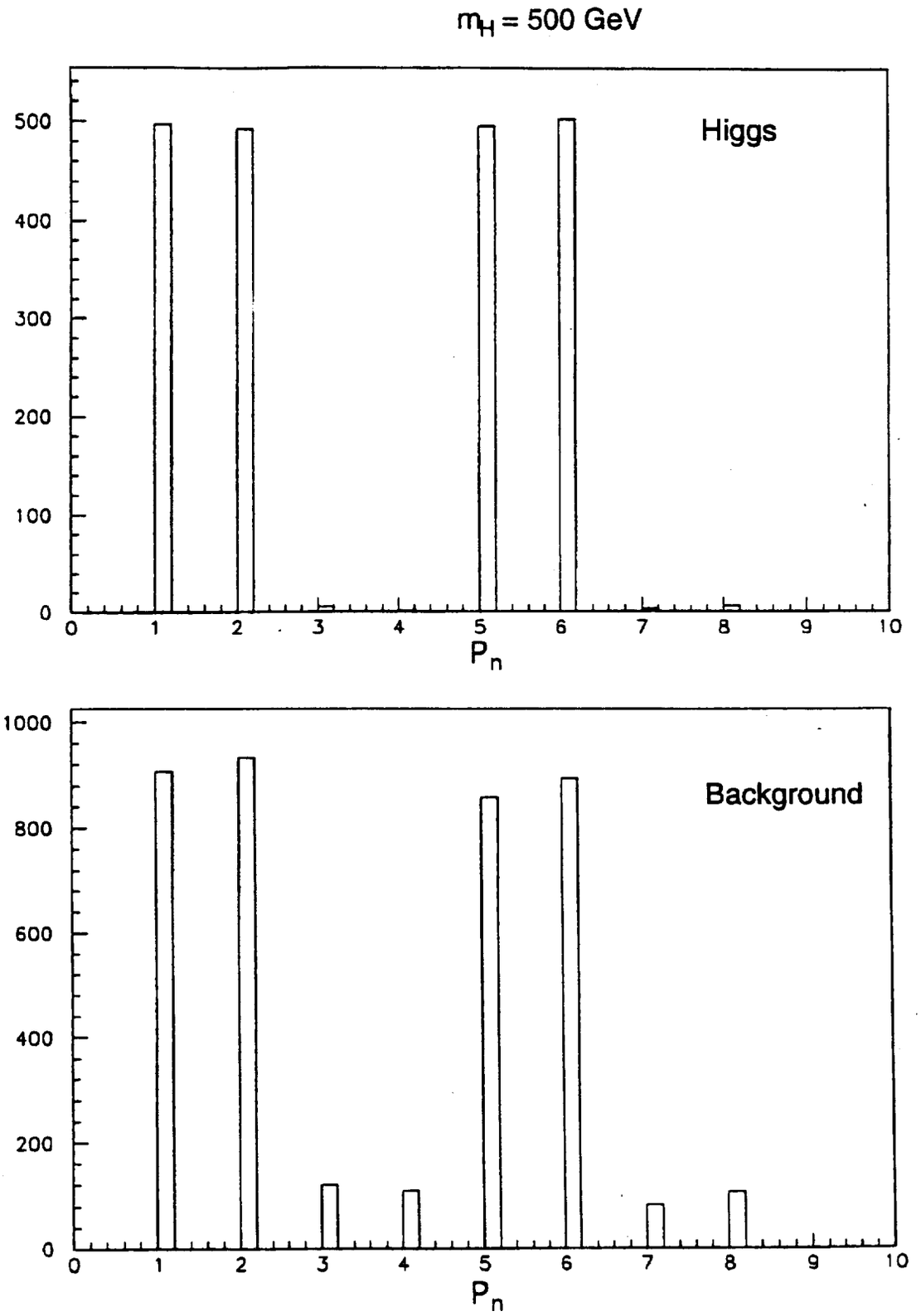

Figure 3b: The combination distribution for Higgs events (top) and background ones (bottom) at $m_H = 500$ GeV/c^2.

The conclusion is that the technique ofthe minimal spanning tree requires a very good ordering of leptons inside the Z bosons.

Using the parameter $N_0 = 30$, 8 clusters for $m_H = 400$ GeV mass interval, and 10 clusters for $m_H = 500$ GeV were selected with populations $N > 100$ event. It is remarkable that these clusters could be separated into two groups: clusters produced mainly by Higgs bosons (Table 2) and clusters with predominant background contamination (Table 3). The content of the H_0 event in the Higgs clusters dominates: 60% at $m_H = 400$ GeV and 55% for $m_H = 500$ GeV.

Table 2: Clusters with $H \rightarrow 2e^+2e^-$ decay

$m_H = 400$ GeV/c^2			$m_H = 500$ GeV/c^2		
Cluster	Higgs	Background	Cluster	Higgs	Background
1	193	187	1	375	326
2	303	237	2	349	269
3	568	290	3	550	451
4	212	117	4	58	48
Total	1276	831	Total	1332	1094

Table 3: Clusters with background

$m_H = 400$ GeV/c^2			$m_H = 500$ GeV/c^2		
Cluster	Higgs	Background	Cluster	Higgs	Background
1	68	329	1	26	403
2	6	219	2	45	247
3	41	185	3	37	320
4	14	162	4	8	121
			5	33	447
			6	52	112
Total	129	895	Total	201	1650

In the background clusters the situation is quite the reverse: 13% and 11% Higgs event contamination, respectively. We emphasise that such an elimination reflects to a considerable degree the inner correlations of leptons from Higgs-boson decay. From Tables 2 and 3 we can seen that in the whole we have lost 29% of the original number of H-bosons with mass 400 GeV, and 23% for 500 GeV. This is probably connected with the low populated clusters ($N_0 < 100$) which for reasons of large statistical fluctuation have not been analysed.

How much the transition of leptons affects the Z-mass distribution can be seen from Figs. 4a and 4b.

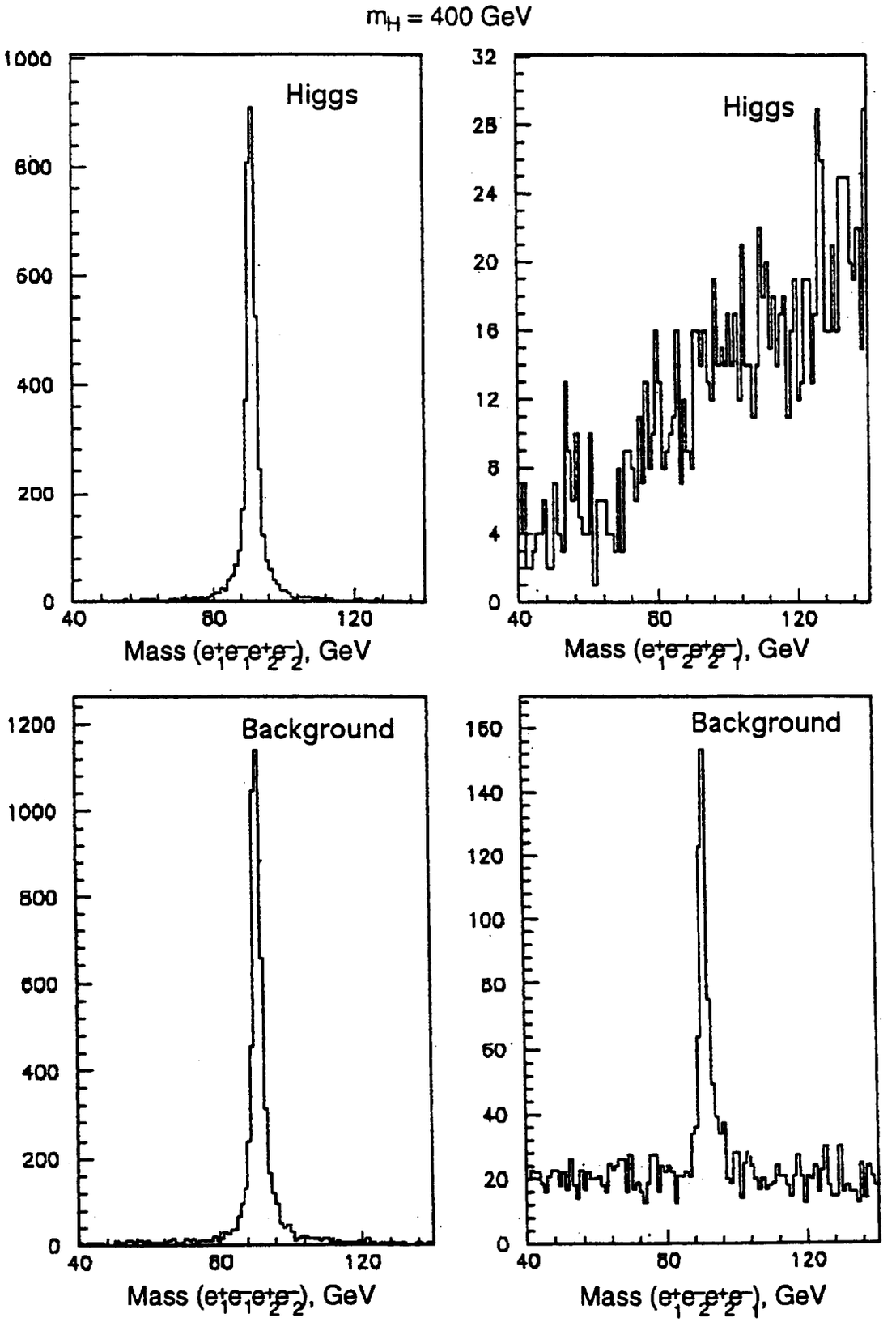

Figure 4a: The invariant mass distribution for different (e^+e^-) combinations of Higgs clusters (top) and background ones (bottom) at $m_H = 400$ GeV/c^2.

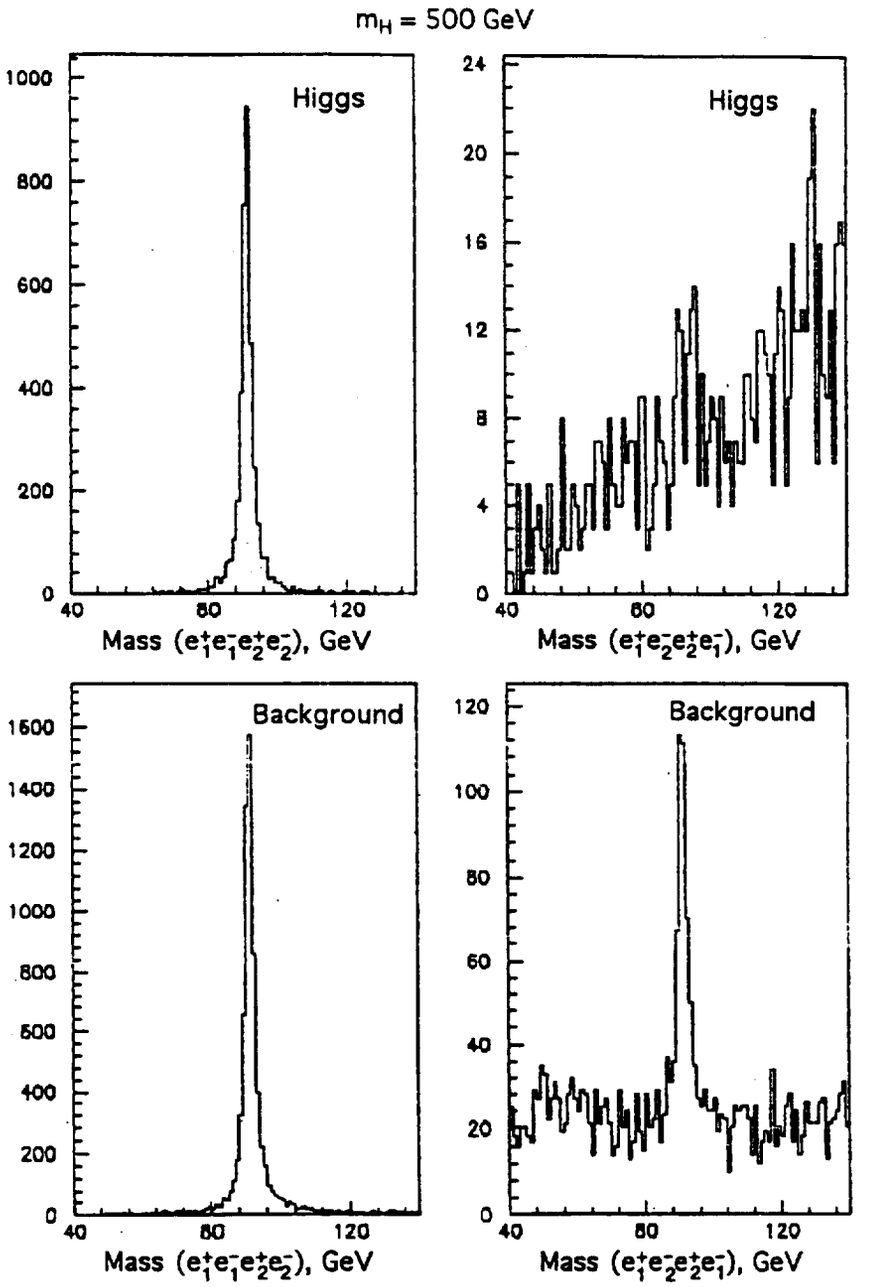

Figure 4b: The invariant mass distribution for different (e^+e^-) combinations of Higgs clusters (top) and background ones (bottom) at $m_H = 500$ GeV/c^2.

For correct ordering it is natural to expect that both the H events and background samples reproduce the original Breit–Wigner resonance distribution. However, under track permutation drastic differences between true and false events appear. In this case, for background events a larger fraction of them was included in the minimal spanning tree and after permutàtions these events gave originally correct masses, but the background masses are uniformely pedestal-like in their distribution. This is additionally a clear indication of the important intrinsic correlations of leptons from Higgs-boson decay.

In Figs. 5a and 5b the 4 lepton $(\ell^+\ell^-\ell^+\ell^-)$ mass distribution is presented for the full statistics: 5000 samples and 6000 samples for $m_H = 400$ GeV, and 500 GeV respectively.

The dashed area corresponds to the events from the Higgs group of clusters and the double dashed the background samples among them. As can be seen, the background contamination is essentially suppressed.

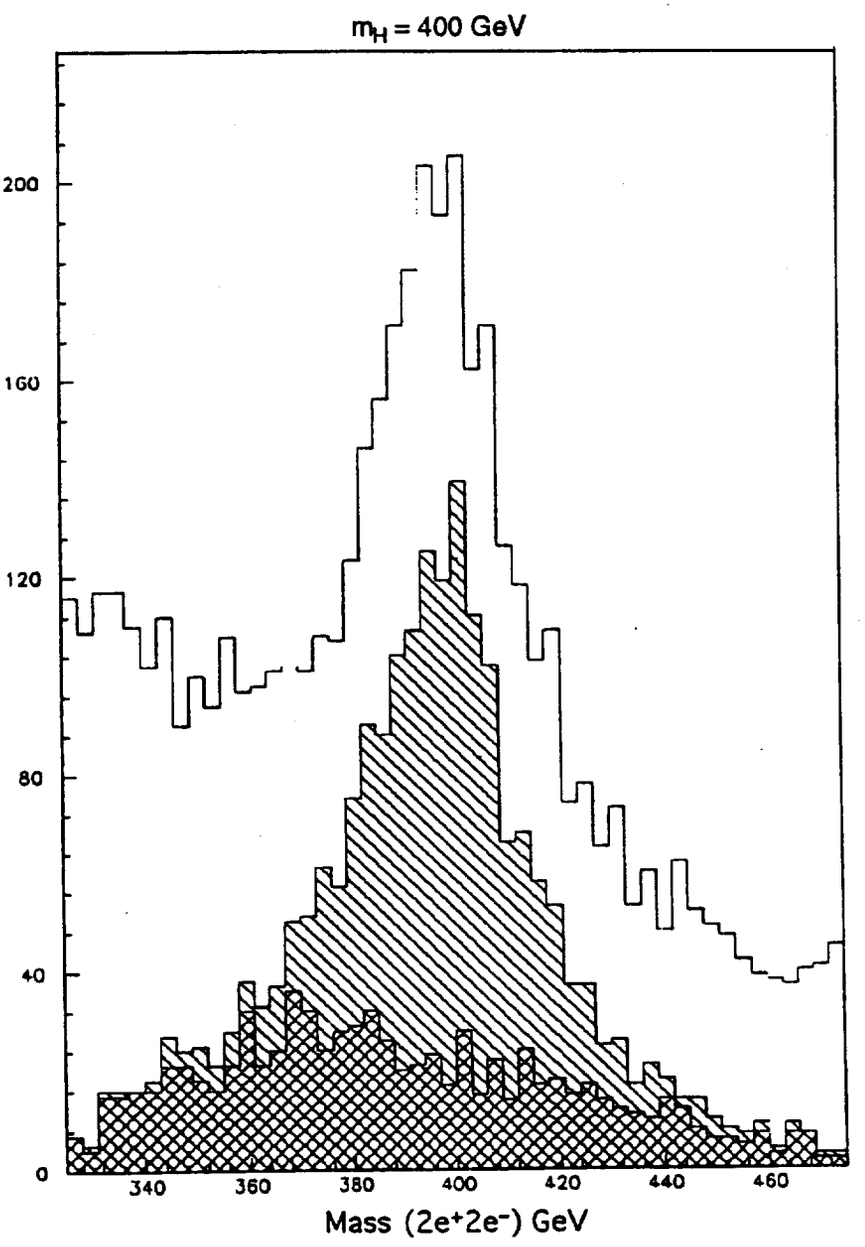

Figure 5a: The invariant mass distributions of the $(2e^+2e^-)$ system for all events, Higgs (dashed area) and background (double dashed area) events from the first group of clusters at $m_H = 400$ GeV/c^2.

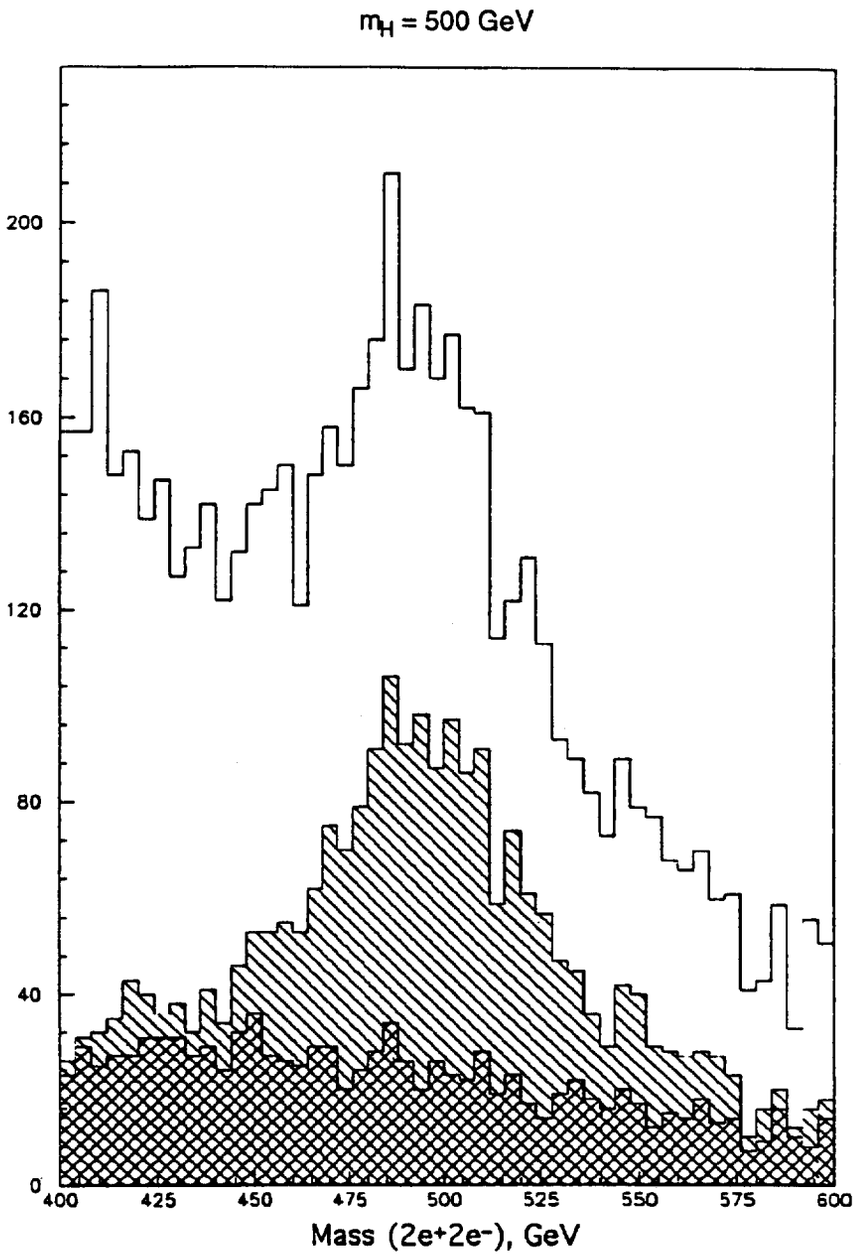

Figure 5b: The invariant mass distributions of the $(2e^{+}2e^{-})$ system for all events, Higgs (dashed area) and background (double dashed area) events from the first group of clusters at $m_H = 500$ GeV/c^2.

In Figs. 6a and 6b the *a priori* given Higgs mass distribution is compared with the events, whose mass was selected from the Higgs clusters. No distortion was found in the mass shape.

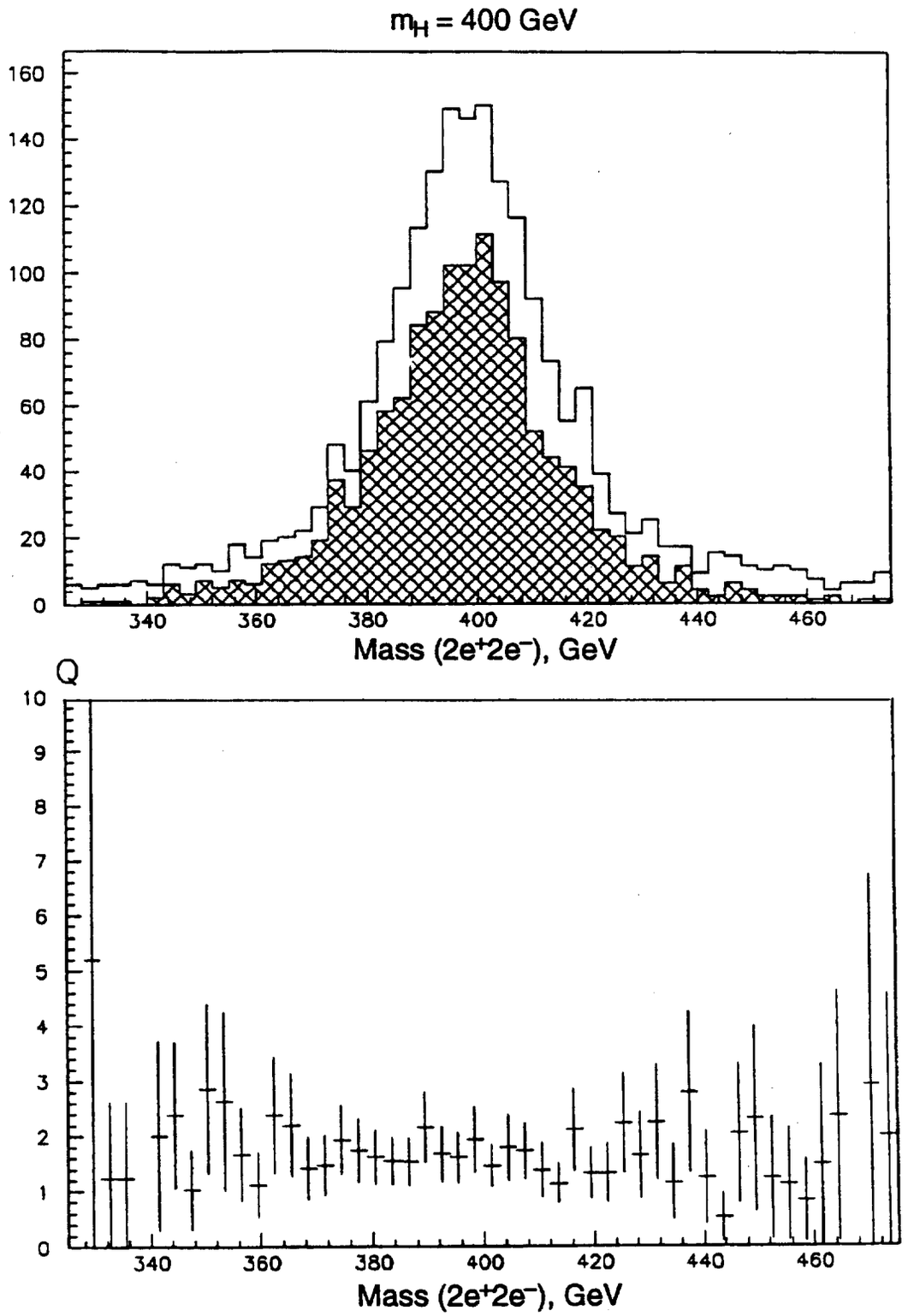

Figure 6a: The spectra of the Higgs boson's invariant mass (top) before and after (double dashed area) separation of the clusters and variation of the Q value (bottom) at m_H = 400 GeV/c^2.

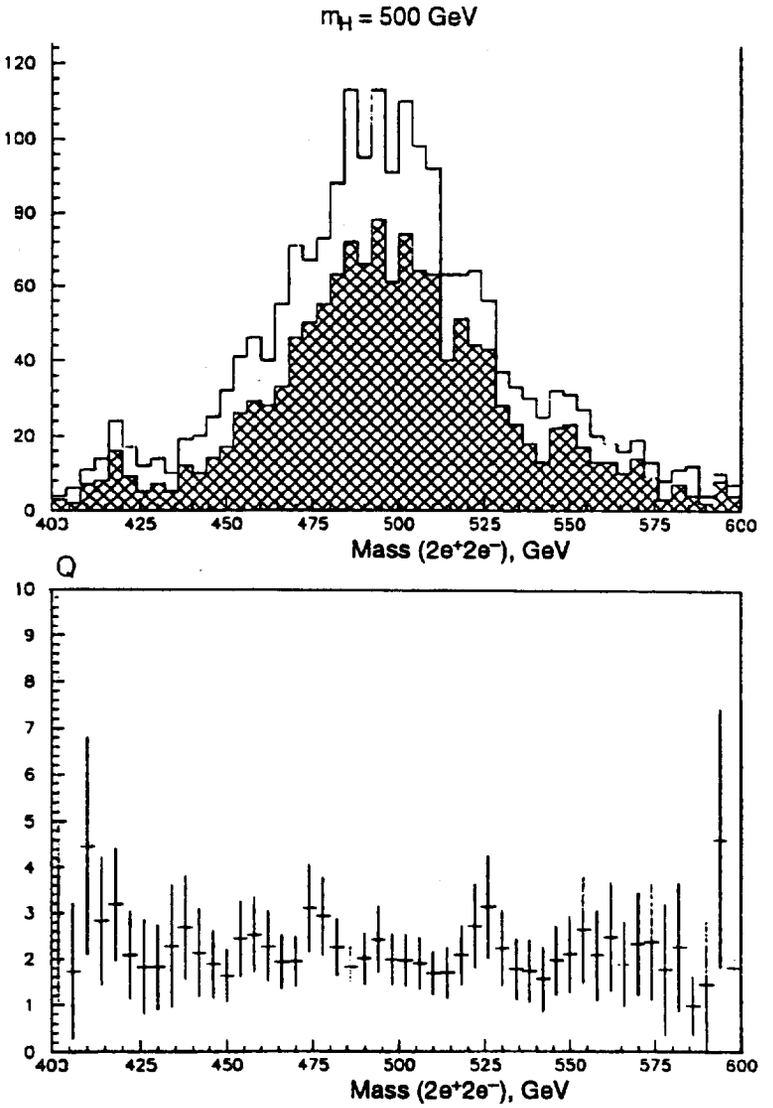

Figure 6b: The spectra of the Higgs boson's invariant mass (top) before and after (double dashed area) separation of the clusters and variation of the Q value (bottom) at m_H = 500 GeV/c^2.

In the bottom part of this figure the relation of signal to background after the clusterization of events compared to the sample before clusterization is given. It can be seen that in the full mass interval this value fluctuates around 2. This indicates that even with such poor initial conditions a considerable cleaning of the analysed sample of events with Higgs production is achieved.

In conclusion, for the 400 GeV mass interval the four-lepton mass spectrum in each individual cluster is given (Fig. 7a for Higgs clusters; Fig. 7b for background clusters): an obvious signal from Higgs-resonance is present in all Higgs-clusters. In contradiction to this the shapes of the mass distribution in each background cluster is qualitatively different. This is a clear indication of the cluster separation in the real ATLAS experiment.

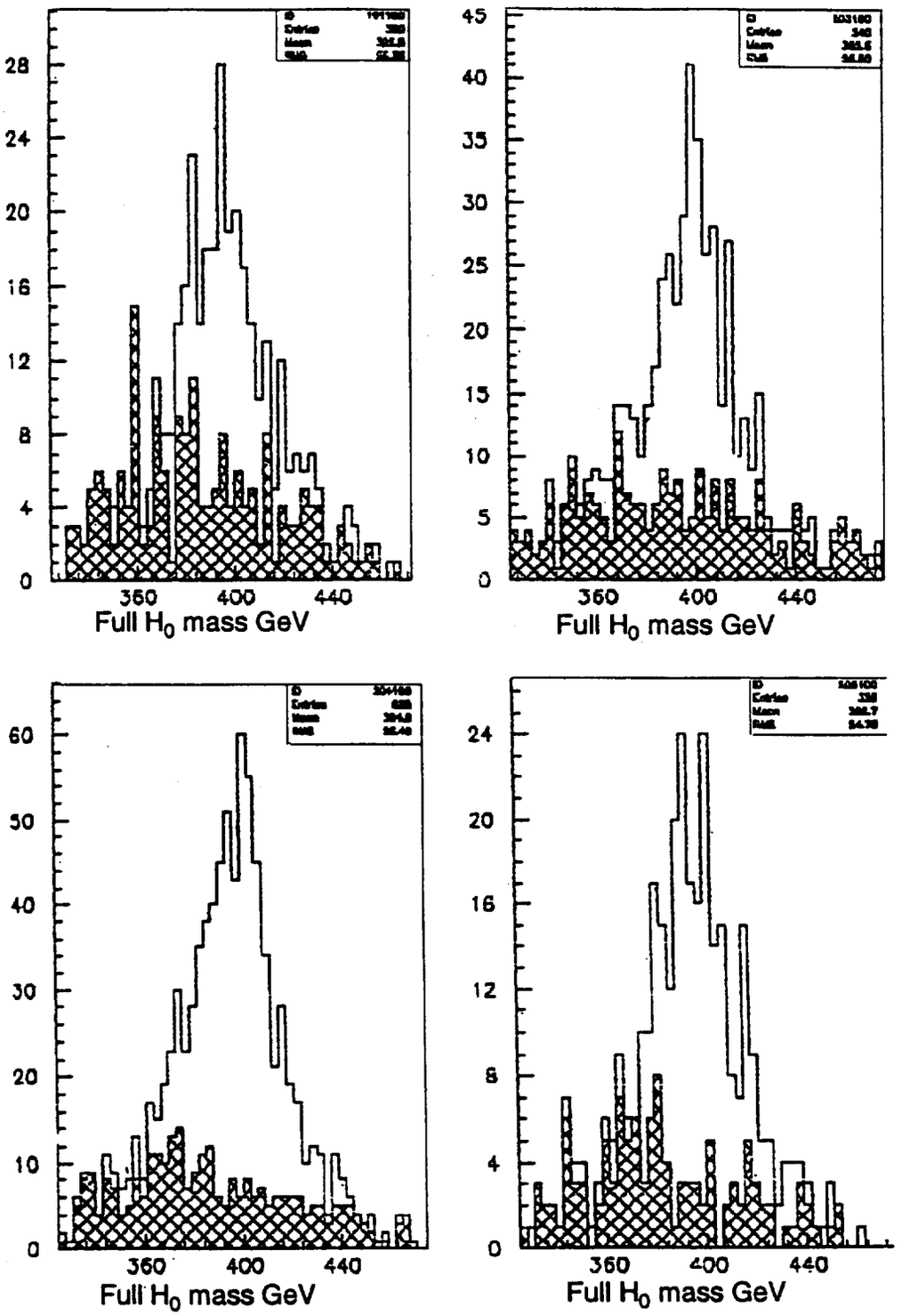

Figure 7a: The invariant mass distribution of the $(2e^+2e^-)$ system in each of the Higgs clusters (Table 2) for the group of events at $m_H = 400$ GeV.

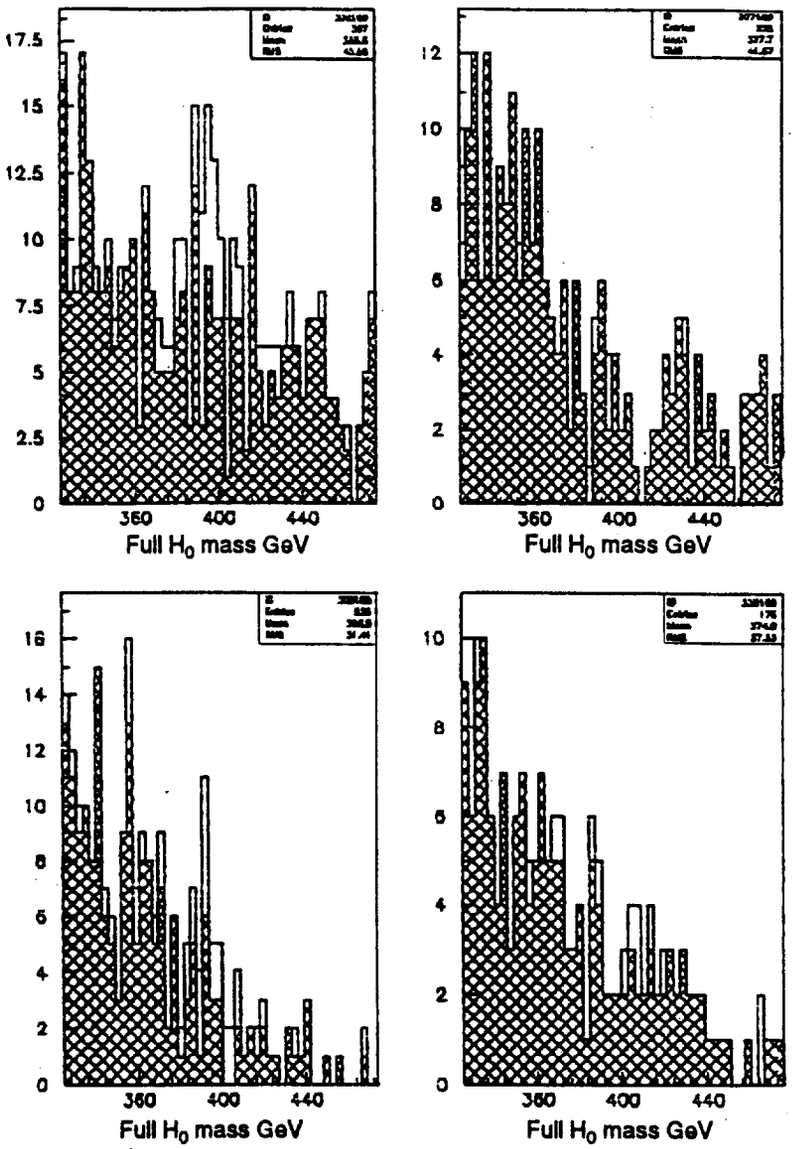

Figure 7b: The invariant mass distribution of the $(2e^+2e^-)$ system in each of the background cluster (Table 3) for the group of events at $m_H = 400$ GeV.

By crossing the number of samples used with the integral luminosity 10^5 pb^{-1} we compare our data with the results received by traditional cuts of transverse momentum $p_\perp$ $(1;2) > 20$ GeV; $p_\perp(3;4) > 7$ GeV and quasirapidity ($|\eta| < 2.5$) of the secondary leptons [16]. As can be seen (Tables 4 and 5), the clusterization method gives the largest number of selected Higgs events with considerable significance:

$$\varepsilon = \frac{N_H}{\sqrt{N_{Bg}}} \pm \delta\varepsilon\,; \qquad \delta\varepsilon = \sqrt{\left(\frac{\partial\varepsilon}{\partial N_H}\right)^2 \sigma^2_{N_H} + \left(\frac{\partial\varepsilon}{\partial N_{Bg}}\right)^2 \sigma^2_{Bg}}$$

$$= \sqrt{\left(\frac{N_H}{N_{Bg}}\right) + \frac{1}{4}\left(\frac{N_H}{N_{Bg}}\right)^2}\,; \qquad \sigma_{N_H} = \sqrt{N_H}\,; \qquad \sigma_{Bg} = \sqrt{N_{Bg}}\,. \tag{16}$$

Table 4: Total number of accepted events for integrated luminosity 10^5 Pb^{-1} for signal $pp \to H_0 \to ZZ \to 4\ell$ and continuim background for $M_H = 400$ GeV, $\sigma_m = 14.2$ GeV [16].

$\Delta M_H = M_H \pm \mathcal{L} \times \sigma_m$							
Methods	Cut	$\mathcal{L}$	ε	N_H	N_{Bg}	$N_H - N_{Bg}$	N_H/N_{Bg}
Clusterisation	$\sigma_m = 14.2$ GeV	5.3	25.7 ± 1.5	429	279	150	1.5
		2.0	32.5 ± 2.2	378	135	243	2.8
		1.64	32.6 ± 2.3	351	116	232	3.0
Traditional cut method (ATLAS Internal Note, Phys. No. 048, March 1995) [16]	$\sigma_m = 14.2$ GeV $\lvert\eta\rvert < 2.5$ $P_\perp(1;2) > 20$ GeV $P_\perp(3;4) > 7$ GeV	2	31.6 ± 1.8	300	91	209	3.3
		1.64	33 ± 2.7	285	74	211	3.9
	$\sigma_m = 14.2$ GeV $\lvert\eta\rvert < 2.5$ $P_\perp(1;2) > 20$ GeV $P_\perp(3;4) > 7$ GeV $P_{\perp z}^{max} > \frac{M_H}{3} = 133$ GeV	2	40.6 ± 4	267	43	224	6.2
		1.64	42.4 ± 4.5	253	35	218	7.2
	$\sigma_m = 14.2$ GeV $\lvert\eta\rvert < 2.5$ $P_\perp(1;2) > 20$ GeV $P_\perp(3;4) > 7$ GeV $P_{\perp z}^{max} > \frac{M_H}{2} = 200$ GeV	2	50.3 ± 11.7	129	6	123	21.5
		1.64	52.6 ± 13.0	122	5	117	24.4

Table 5: Total number of accepted events for integrated luminosity 10^5 Pb^{-1} for signal $pp \to H \to ZZ \to 4\ell$ and continum background for $M_H = 500$ GeV, $\sigma_m = 28.7$ GeV [16].

$\Delta M_H = M_H \pm \mathcal{L} \times \sigma_m$							
Methods	Cut	$\mathcal{L}$	ε	N_H	N_{Bg}	$N_H - N_{Bg}$	N_H/N_{Bg}
Clusterisation	$\sigma_m = 28.7$ GeV	3	15.6 ± 1.3	200	164	36	1.22
		2	17.6 ± 1.6	176	100	76	1.76
		1.64	17.8 ± 1.7	163	84	79	1.94
Traditional cut method (ATLAS Internal Note, Phys. No. 048, March 1995) [16]	$\sigma_m = 28.7$ GeV $P_\perp(1;2) > 20$ GeV $P_\perp(3;4) > 7$ GeV $\lvert\eta\rvert < 2.5$	2	21.3 ± 2.7	154	52	102	3.0
		1.64	22.4 ± 2.2	145	42	103	3.3
	$\sigma_m = 28.7$ GeV $P_\perp(1;2) > 20$ GeV $P_\perp(3;4) > 7$ GeV $\lvert\eta\rvert < 2.5$	2	29.2 ± 4.0	137	22	115	6.2
		1.64	22.4 ± 2.2	145	42	103	3.3
	$\sigma_m = 28.7$ GeV $P_\perp(1;2) > 20$ GeV $P_\perp(3;4) > 7$ GeV $\lvert\eta\rvert < 2.5$ $P_{\perp_z}^{max} > \frac{1}{3}M_H = 167$ GeV	2	29.2 ± 4.0	137	22	115	6.2
		1.64	30.6 ± 4.5	130	18	112	7.2
	$\sigma_m = 28.7$ $P_\perp(1;2) > 20$ GeV $P_\perp(3;4) > 7$ GeV $\lvert\eta\rvert < 2.5$ $P_{\perp_z}^{max} > \frac{M_H}{2} = 250$ GeV	2	39.8 ± 12.4	69	3	66	23
		1.64	46 ± 17.3	65	2	63	32.5

By increasing the selection criterion in the traditional cut method $P_{\perp_e}^{max} > \frac{M_H}{3}$ or $P_{\perp_e}^{max} > \frac{M_H}{2}$) an improved significance was reached, but its reliability essentially drops.

Once again we wish to emphasise the importance of the interior lepton correlations in the $H \rightarrow ZZ \rightarrow 4\ell$ decays. This feature must be considered by combining the traditional kinematic and electronic cuts with the produced method. For smaller Higgs masses and hence a smaller width of the state we expect a stronger correlation of the decay products. Our method should therefore permit an improved background rejection.

The authors would like to thank P. Jenni, D. Froidevaux, C. Fabjan and D. Fournier for helpful discussions.

References

[1] G. Arnison et al., (UA1 Collab.), Phys. Lett. **122B** (1983) 103;
M. Banner et al., (UA2 Collab.), Phys. Lett. **122B** (1983) 476;
G. Arnison et al., (UA1 Collab.), Phys. Lett. **126B** (1983) 238;
P. Bagnaia et al., (UA2 Collab.), Phys. Lett. **129B** (1983) 130.

[2] H.B. Jensen, Proc. 27th Int. Conf. on High Energy Physics, Vol. 1 (1994) p. 3;
P.D. Grannis, Proc. 27th Int. Conf. on High Energy Physics, Vol. 1 (1994) p. 15.

[3] L. Okun, Leptons and Quarks, Moskow 'Nauka', 1991.

[4] S. Cortese and P. Petronzio, Phys. Lett. **B276** (1992) 203;
A. Dobado, V.I. Herrero, I. Perron, Z. Phys. **C50** (1991) 205.

[5] M.Z. Akrawy et al., CERN-PPE/90-150 (1990);
D. Decamp et al., CERN-PPE/90-101 (1990).

[6] S.M. Errede, Proc. 27th Int. Conf. on High Energy Physics, Vol. 2 (1994) p. 433.

[7] P. Abren et al., CERN preprint CERN-PPE/40-163 (1990).

[8] G. Altarelli et al., Proc. Workshop on Physics at Future Accelerators, La Thuile and Geneva, 1987, ed. J. Mulrey, CERN 87-07, Geneva 1987, Vol. 1, p. 36;
D. Froidevaux et al., ibid., p. 61;
M. Spizta et al., DESY 94-123; GPP-Udem-TH-95-16, CERN-TH/95-30.

[9] I.F. Gunion et al., The Higgs Hunter's Guide (Addison-Westley, Mento Park, California, 1989).

[10] E.G. Boos et al., Yad. Fiz., Vol. 54, vyp. 2 (8) (1991) p. 538.

[11] E.W. Dijkstra, A discipline of programming (Englewood Cliff, Prentice-Hall, 1976).

[12] T. Ludlam, R. Slansky, Phys. Rev. D, Vol. 16 (1977) p. 100.

[13] K. Fukunaga and L.D. Hostetler, IEEP Trans. Inf. Theory IT-19, **320** (1973).

[14] R. Horn, Ch. Johnson Matrix analysis (Cambridge University Press, 1986).

[15] T. Sjöstrand, CERN-TH.7112/93.

[16] ATLAS Internal note, Phys-No-48 March 1995: E. Richter-Was et al.